

Tannic complexes coated nanocontainers for controlled release of corrosion inhibitors in self-healing coatings

Bei Qian^{1, 2}, Marios Michaiidis², Matt Bilton³, Theo Hobson², Zhaoliang Zheng², Dmitry Shchukin^{2, 4*}

1. College of Chemistry and Pharmaceutical Sciences, Qingdao Agricultural University, 700 Changcheng Road, Qingdao 266109, PR China

2. Stephenson Institute for Renewable Energy, Department of Chemistry, University of Liverpool, Crown Street, Liverpool L69 7ZD, U.K.

3. Imaging Centre at Liverpool, University of Liverpool, Liverpool L69 3GL, U.K.

4. Northwestern Polytechnical University, Xi' An, China.

Corresponding author: Prof. Dmitry Shchukin

Stephenson Institute for Renewable Energy, Department of Chemistry, University of Liverpool, Crown Street, Liverpool L69 7ZD, U.K.

E-mail: D.Shchukin@liverpool.ac.uk

Tel.: 0044-151-7952304

Abstract

Nanocontainers with controlled release properties have been used in self-healing coatings for many years. However, the spontaneous leakage of the small molecular weight inhibitors from the nanocontainers promoted the development of nanovalves or gatekeepers to control inhibitor release. Herein, we demonstrate a facile method to encapsulate corrosion inhibitor in mesoporous silica nanoparticles (MSNs) with the help of tannic acid complexes, which endow the inhibitor loaded MSNs with pH-controlled release function. Commercial water-borne alkyd coating impregnated with 2 wt% of benzotriazole-loaded nanocontainers presented significant self-healing effect after 20 days of immersion in 0.1 M NaCl solution from both released benzotriazole and tannic acid as confirmed by electrochemical impedance spectroscopy and microscopy. The impedance modulus of coating with nanocontainers increased from $4.7 \times 10^4 \Omega \text{ cm}^2$ to $1.8 \times 10^5 \Omega \text{ cm}^2$ after 15 days of immersion.

Keywords

Self-healing; Tannic acid; Mesoporous silica; Corrosion protection

1. Introduction

Encapsulation of small molecules such as drugs or corrosion inhibitors in mesoporous nanoparticles is under research attempts during last decade [1-8]. The fast leakage of such molecules from the nanocontainers promoted the development of nanovalves or gatekeepers, which serve as an intelligent shell on the surface of nanocontainers, making it possible to release cargos on demand only. Local pH changes are the most studied trigger as it can be induced by the corrosion process. Bioinspired nanovalves prepared from metal precipitates and supramolecular complexes have been proven to be an appropriate gatekeeper for the nanocontainers [5, 9-11]. Besides their high cost, the major drawback of these nanovalves is single function, which only served as the pH-controlled release gatekeeper.

Mussel-inspired polydopamine (PDA) coatings have attracted tremendous interests due to several advantages including (i) simple ingredients and mild reaction conditions needed for self-polymerization, (ii) ability to graft on a variety of surface from organic to metal materials, (iii) secondary surface modification benefit a wide range of applications, and (iv) pH-sensitive properties of PDA [12-15]. However, there are two main disadvantages to be addressed before PDA finds usage in self-healing coatings. Considerably long times are required for PDA assembly process, usually over 12 h [16, 17]. It has been reported that the benzotriazole (BTA, a commonly used corrosion inhibitor) entirely release from the mesoporous silica nanoparticles in 0.5 h [2], which indicates that the loaded inhibitors will all leak away before the formation of PDA. Ultrafast PDA surface modification by using an oxidizing agent such as NaIO_4 will be difficult to find practical applications while considering safety and environmental pollutions [18, 19]. Another issue is the high cost of dopamine (4.25 GBP/g, Sigma-Aldrich, UK).

Recently, thin films formed by tannic acid (TA) and Fe^{3+} were reported by Hiroataka Ejima et al. [20]. TA is a class of non-toxic, biodegradable polyphenol compound (as shown in Fig. 1) usually extracted from the barks of trees, which has been historically used for preventing corrosion [21-23]. Compared with the long time needed for PDA film formation, the deposition of coordination complexes between TA and Fe^{3+} on a range of planar surfaces can be completed instantaneously in 20 s. Besides, the low-cost raw materials (0.13 GBP/g for tannic acid, 0.04 GBP/g for FeCl_3 , Sigma-Aldrich, UK) will make it easily be enlarged to industrial scale.

Herein, we developed an extremely quick deposition shell on the surface of nanocontainers used for self-healing coatings. Coordination complexes of TA and Fe^{3+} ion terminate spontaneous leakage of inhibitors at the neutral pH and provide an additional protective effect for the coatings. Despite a large number of the literature devoted to analysis the scratched area of coatings [24-28], only a few attempts have been made to study the coating apart from the scratched area such as the micropores of the coating. In this paper, we mainly focused on the design of multifunctional gatekeepers on the surface of MSNs.

2. Experimental

2.1. Materials.

Tetraethyl orthosilicate (TEOS, 98%), hexadecyltrimethylammonium bromide (CTAB, 99%), triblock copolymer F127 (Pluronic F127), ammonium hydroxide (32%), ethanol (99.8%), 1H-benzotriazole (BTA), tannic acid (TA), and iron (III) chloride were purchased from Sigma-Aldrich UK. The mild steel samples were supplied by The Metal Store, UK. The water-based alkyd coating was provided by Crown Trade, UK.

2.2. Nanocontainers.

The mesoporous silica nanoparticles (MSNs) with a branched 3D structure were fabricated according to the method reported in Ref [29]. The detailed fabrication process is described in Supporting Information section. Before encapsulation, the as-prepared MSNs were dried at 120 °C under vacuum for 12 h to acquire unblocked mesoporous structure. Then, 30 mg of MSNs were mixed with 30 ml of BTA saturated solution in ethanol. The mixed solution was evacuated using a vacuum pump to obtain the maximum loading of the inhibitor. During the encapsulation, bubbles can be observed on the top of the mixed solution as shown in Figure S2. The as-loaded MSNs (MSN-BTA) are removed by centrifugation for 10 min at 10000 rpm. TA-Fe (III) complex (TAC) shell was deposited on the surface of MSN-BTA applying the procedure introduced by Hirota et al. [20]. FeCl₃ and then TA solutions were added to the MSN-BTA suspension. Their final concentrations were 10 mg/mL of MSN-BTA, 0.1 mg/mL of FeCl₃, and 0.4 mg/mL of TA respectively. The suspension was vigorously mixed by a vortex mixer for 20 s immediately after the addition of TA. The TAC coated MSN-BTA particles (MSN-BTA@TAC) were separated by centrifugation and washed with water to remove excess TA and FeCl₃. The preparation process is shown in Fig. 1.

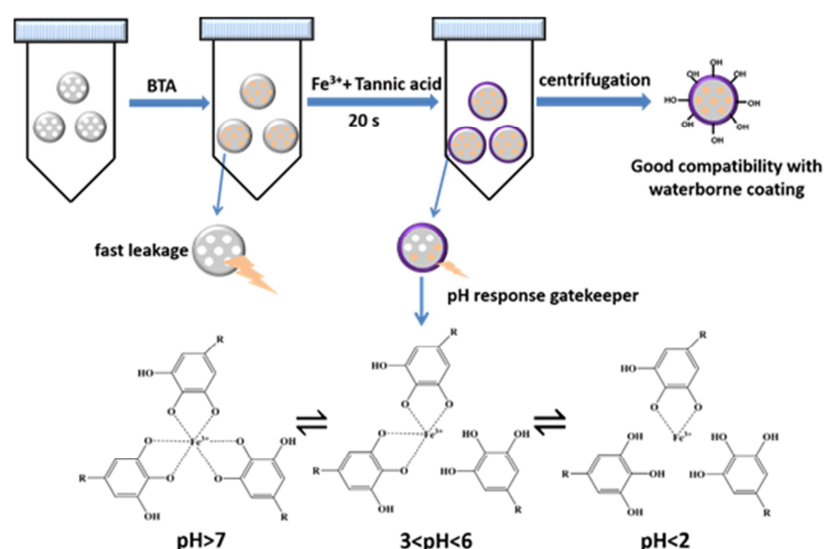


Fig. 1. Synthesis of MSN-BTA@TAC and its pH-triggered mechanism.

2.3. Coatings

MSN-BTA@TAC (2 wt%) was added to the alkyd paint emulsion. After that, the mixed matrix was mechanically stirred via a homogenizer for five minutes. It is worth note that stirring for a longer time will cause the heating of the alkyd matrix, which may result in the curing of the coating. Paints without MSNs (blank coating), with 2 wt% MSNs, and 2 wt% MSN-BTA were prepared the same way. The samples were deposited on the mild steel plates using a paint applicator (PK Paint Applicator, UK) and dried at room temperature for 48 h. Figure S3 shows the coated samples after drying.

2.4. Characterization.

The release profiles of BTA were detected according to the method described in our previous work [9]. Fluorescence spectroscopy (LS 55 Fluorescence Spectrometer, PerkinElmer) was chosen to exam the release profiles of BTA because of its higher selectivity and sensitivity as compared to UV-visible spectroscopy. Excitation was performed at 275 nm to get the appropriate fluorescence signal from BTA. No fluorescence signals can be acquired from the tannic acid, Fe^{3+} , or their complex excited at 275 nm. The emission maximum of BTA at 364 nm was plotted as a function of release time.

Electrochemical impedance spectroscopy (EIS) measurements, which can disclose the fundamental processes of corrosion at defects and underneath coatings [30], were taken to monitor the corrosion behaviour of the self-healing coating. Mild steel substrates (3 cm × 6 cm × 0.3 cm) with coatings were placed into specially designed cells. The electrolyte was fixed in a glass tube by an O-ring as shown in Figure S4. The coated mild steel with an exposed area of 4 cm² was used as the working electrode, a platinum sheet was used as the auxiliary electrode, and Ag/AgCl (3 M KCl) electrode was used as the reference electrode. Scratches were made with a circular-edge scalpel by a home-made machine as shown in

Figure S5. The corrosive electrolyte was 0.1 M NaCl solution. Open circuit potential (OCP) was measured for 30 min following EIS measurements over the frequency from 10^5 Hz to 10^{-2} Hz using an AC signal amplitude of 10 mV at OCP. After 20 days of immersion, all scratched coatings were tested by potentiostatic polarisation. The Tafel plots were obtained with a 1 mV/s scan rate and at a potential range between -300 mV and +300 mV versus OCP. All electrochemical tests were performed three times to guarantee the repeatability of each experimental condition. Data were fitted to equivalent cell diagrams using the IviumSoft program.

3. Results and discussion

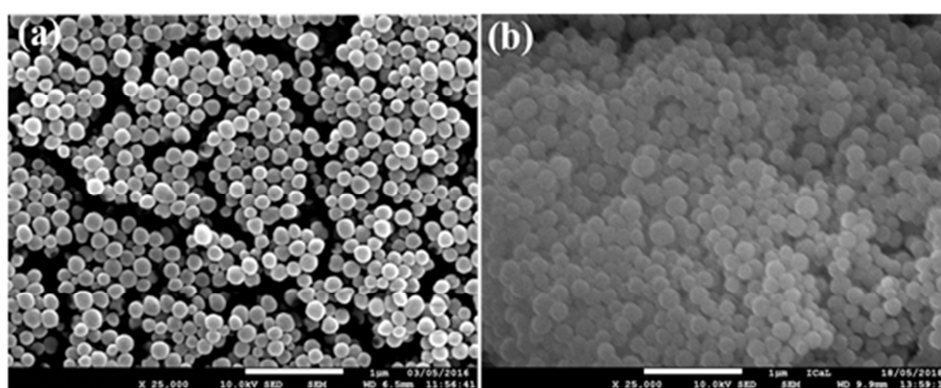


Fig. 2. SEM images of MSNs (a) and MSN-BTA@TAC (b) Scalebar is 1 µm for both images.

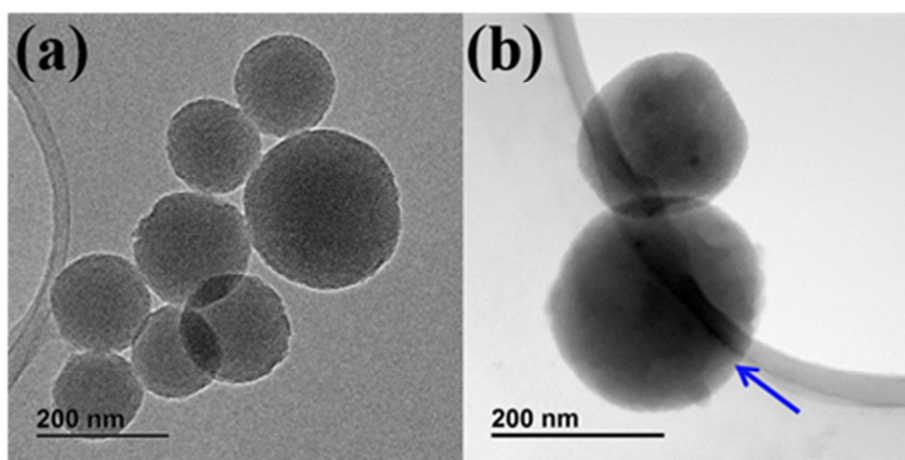


Fig. 3. TEM images of MSNs (a) and MSN-BTA@TAC (b).

Fig. 2 (a, b) shows the SEM images of MSNs and MSN-BTA@TAC. Both samples have spherical shape with the size range from 70 nm to 200 nm. TEM analysis was performed to follow the variation of nanoparticle morphology before and after encapsulation. It can be seen from Fig. 3 (a) that the well-ordered worm-like pores are extending over the whole structure of the MSNs. After the encapsulation and TAC coating, the diameter of MSN-BTA@TAC is bigger than that of initial MSNs (Fig. 3 (b)). A rough film can be clearly seen on the surface of MSN-BTA@TAC.



Fig. 4. Pictures of MSNs (a), MSN-BTA (b), and MSN-BTA@TAC (c).

Fig. 4 shows the visual pictures of MSNs, MSN-BTA, and MSN-BTA@TAC. The pristine nanoparticles (Fig. 4 a) are white color power. As compared to the MSNs, MSN-BTA (Fig. 4 a and b) reveals no change in appearance. In contrast, after modification of TAC, the white color became light blue (Fig. 4c).

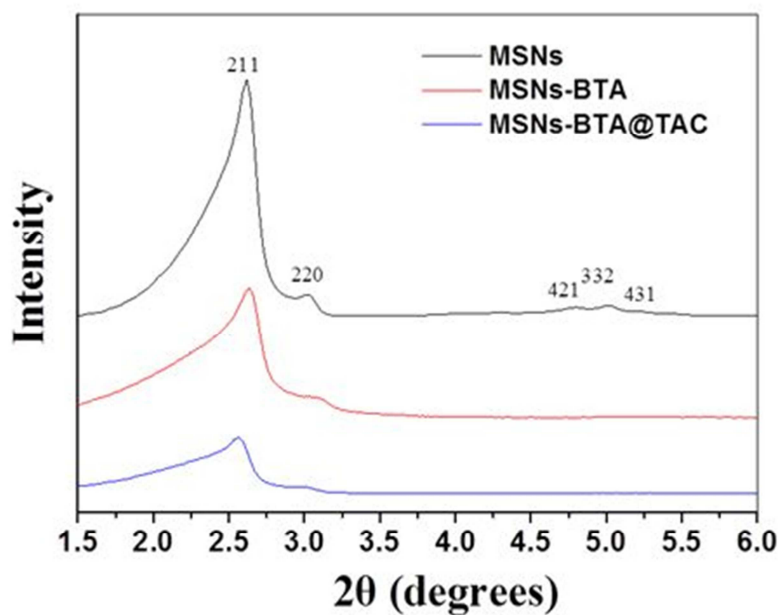


Fig. 5. XRD patterns for MSNs (black), MSN-BTA (red), and MSN-BTA@TAC (blue).

In order to evaluate structural features of the nanoparticles and nanocontainers, powder XRD patterns were recorded for MSNs, MSN-BTA, and MSN-BTA@TAC. The XRD results are shown in Figure 5. Five peaks can be observed from the XRD pattern of MSNs (black line), which correspond to the planes (211), (220), (420), (332) and (431) of MCM-48 [29]. Compared with MSNs, the XRD patterns of MSN-BTA (red line) and MSN-BTA@TAC (blue line) show reduced peaks intensity. All XRD diffraction patterns are able to index to cubic Ia3d mesophase, which indicates that the mesoporous structure is still maintained after BTA encapsulation and TAC deposition on the surface of MSNs.

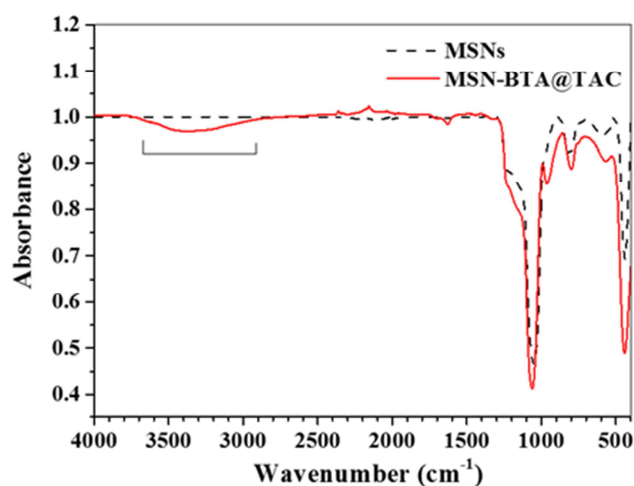


Fig. 6. FTIR spectra of MSNs (black) and MSN-BTA@TAC (red).

Figure 6 demonstrates the FTIR spectra of MSNs and MSN-BTA@TAC. The absorption peaks at 465 cm^{-1} , 800 cm^{-1} and 1080 cm^{-1} correspond to Si-O-Si bending vibration, Si-O-Si symmetric stretching, and Si-O asymmetric vibration, respectively. All these peaks are characteristic peaks for SiO₂ [31]. The most significant difference between MSNs and MSN-BTA@TAC is the broad absorption band between 3700 cm^{-1} and 2700 cm^{-1} implying the presence of polyphenols [32]. The above results confirm the successful deposition of TAC on the surface of MSNs.

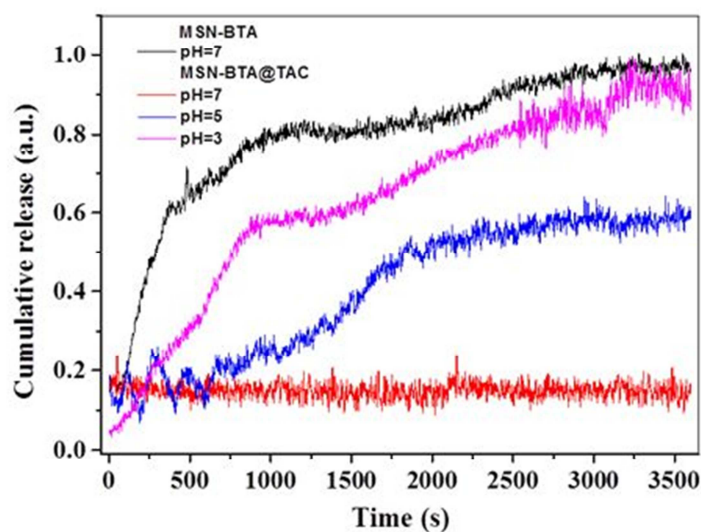


Fig. 7. Release profiles of BTA from the MSN-BTA and MSN-BTA@TAC at different pH determined by fluorescence spectra.

The pH sensitivity of MSN-BTA@TAC nanocontainers was confirmed by fluorescence analysis. Fig. 7 shows a fast release of BTA from MSN-BTA (black line), implying a spontaneous release without the gatekeeper. At pH = 7, more than 80 % of the loaded inhibitor was released in 1500 s from MSN-BTA, which was similar to the results reported by Borisova et al. [2]. On the contrary, a flat baseline between 0.1 and 0.2 a.u. can be seen from Fig. 6 for MSN-BTA@TAC at pH 7, which indicates the complex formed by Fe^{3+} and TA acts as effective nanovalves for BTA. Different trends are observed at pH 5 and pH 3 as shown in Fig. 6. More than 50% of the loaded inhibitor was released from the MSN-BTA@TAC at pH 5 after 1800 s. In the case of pH 3, the release process can be divided into three stages. During the initial fast release stage from 0 s to 750 s, the cumulative release of BTA reached 55%. In the second stage from 750 s to 2000 s, the cumulative release of BTA increased from 55% to 70%. Although it is difficult to assess the release amount on the last stage from 2000 s to 3600 s due to a noisy signal, we can confirm that the release is nearly 90%. It has been reported that the TAC films would become thinner and rougher in the acidic

environment [18]. Our release profiles also confirm that the coordination between Fe^{3+} and TA is pH dependent. The dissociated complexes at lower pH might provide a passage for the as-loaded BTA to release.

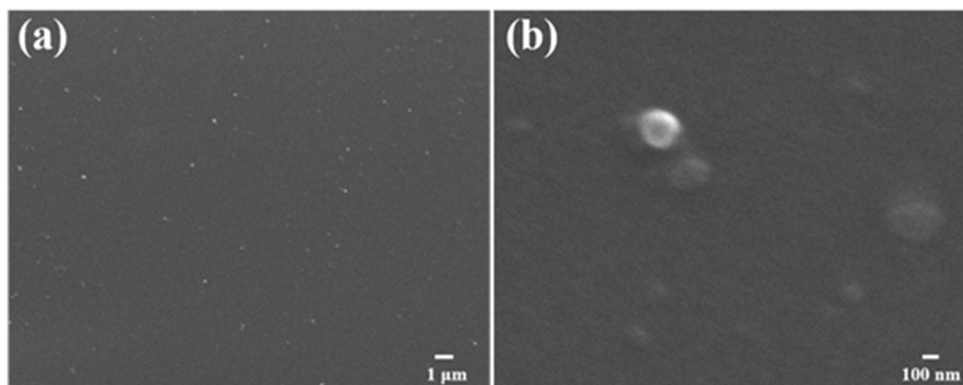


Fig. 8. Cross-section SEM images of coating with MSN-BTA@TAC (a) 5×10^3 magnitude, (b) 5×10^4 magnitude.

SEM cross-sectional images of coatings give us detailed information about the dispersion of nanocontainers. As shown in Fig. 8 (a), small white spheres, which are silica nanocontainers, are homogeneously dispersed in the coating. Nanocontainers without large aggregates can be observed in Fig. 8 (b). Also, no bubbles or cracks can be seen in Fig. 8, implying good compactness of the coating and its compatibility with nanocontainers.

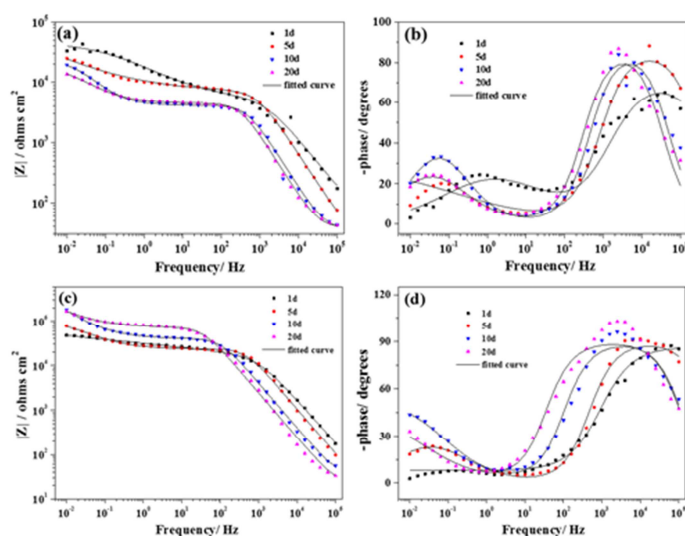


Fig. 9. Bode plots of the scratched coatings during 20 days immersion: blank coating (a, b), coating with MSN-BTA@TAC (c, d).

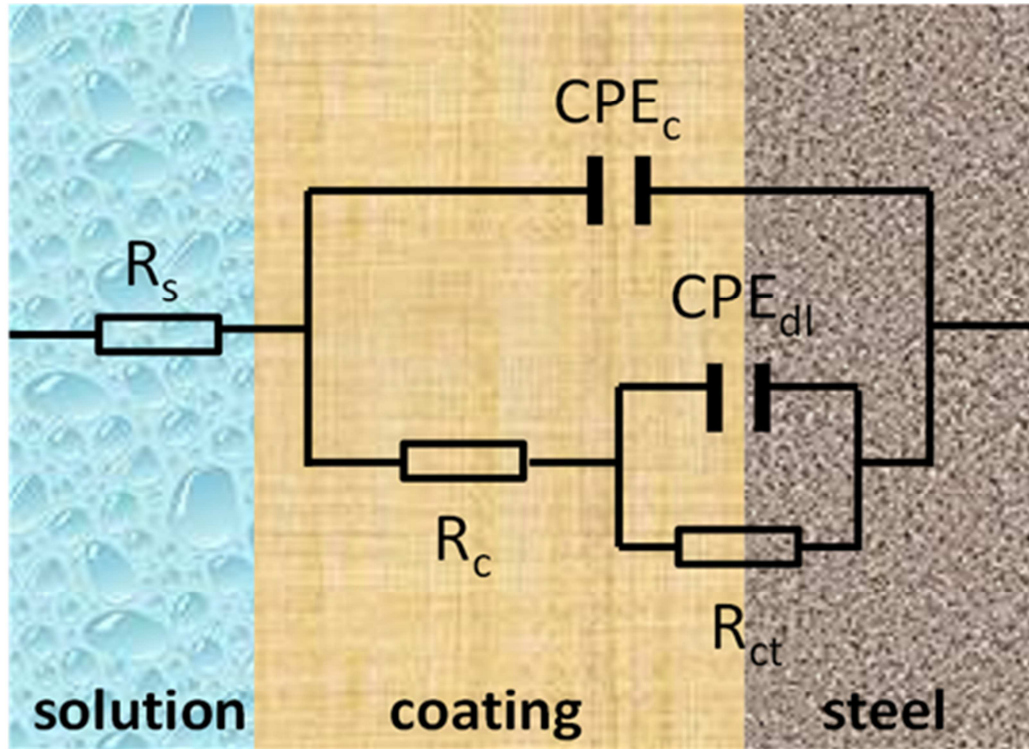


Fig. 10. Electrical equivalent circuit used to fit the impedance data: R_s stands for solution resistance; R_c stands for coating resistance; CPE_c stands for constant phase element of coating capacitance; R_{ct} stands for charge transfer resistance; CPE_{dl} stands for constant phase element of double layer.

Table 1. Electrochemical parameters for blank coating and coating with MSN-BTA@TAC.

coatings	time (day)	R_s ($\Omega \text{ cm}^2$)	CPE_c ($\mu\text{F cm}^{-2}$)	n --	R_c ($\Omega \text{ cm}^2$)	CPE_{dl} ($\mu\text{F cm}^{-2}$)	n --	R_{ct} ($\Omega \text{ cm}^2$)
blank	1	37.22	0.11	0.8132	6935	23.66	0.7758	40510
	5	23.95	0.34	0.9708	5830	136.60	0.7834	27109
	10	35.88	0.87	0.9358	4364	255.70	0.7564	22020
	20	38.43	1.12	0.9635	4032	341.90	0.7632	16630
with MSN-BTA@TAC	1	28.33	0.07	0.9626	11230	27.14	0.8253	25930

5	17.24	0.04	0.9991	23290	58.39	0.8101	97870
10	33.64	0.02	0.9812	39870	36.53	0.8133	112700
20	21.95	0.01	0.9994	71180	38.53	0.8108	116100

Figure 9 demonstrates the Bode plots of the scratched coatings. Considered the overall stability of scratched water-borne alkyd coatings, 20 days was long enough to provide a detailed characterisation of coating performance. Impedance spectra for defected coating were fitted to the electrical equivalent circuit (EEC) shown in Fig. 10. The related fitted data for EIS can be seen from Table 1. In the EEC, R_s stands for the solution resistance. R_c stands for the coating resistance, which is formed by the ionically conducting paths in the matrix. Constant phase element (CPE) was used instead of capacitance to give a better fitting to these depressed semicircles. R_{ct} is the charge transfer resistance at the steel surface, and CPE_{dl} is the double layer capacitance. Fig. 9 (a) shows the variations of Bode plots for blank coating. We can see that the resistance part both in the intermediate frequency (10^1 - 10^3 Hz) and low frequency (10^{-2} - 10^{-1} Hz) areas decreased steadily for 20 days. The time-dependence appearance at low frequencies indicates the corrosion process appeared on the surface of the mild steel. On the contrary, the Bode plots for coating with MSN-BTA@TAC demonstrated positive tendency during 20 days of immersion. The impedance modulus at 0.01 Hz increased from $4.7 \times 10^4 \Omega \text{ cm}^2$ to $1.8 \times 10^5 \Omega \text{ cm}^2$ after 15 days immersion. From then on, it stayed the same until the end of our test. These results indicate the protective effect of the BTA released in the scratched area. The release starts at the beginning of corrosion process due to the local pH changes. The resistive plateau at the intermediate frequency slightly decreased in the first five days and then increased rapidly until the end of the test. During the first few days, there is no corrosion happen in the micropores of the coating. After five days of immersion, the substrate exposed to corrosive species through the formed conductive paths. Then the TA

detaches from the surface of MSNs providing additional protective effect by consuming the reactive rust or forming complexes with Fe^{3+} . As the controlled samples, the EIS results of coatings with 2 wt% MSN and 2 wt% MSN-BTA displayed no autonomous self-healing functionality. Figure 11 shows the evolution of R_{ct} for blank coating and coating with MSN-BTA@TAC.

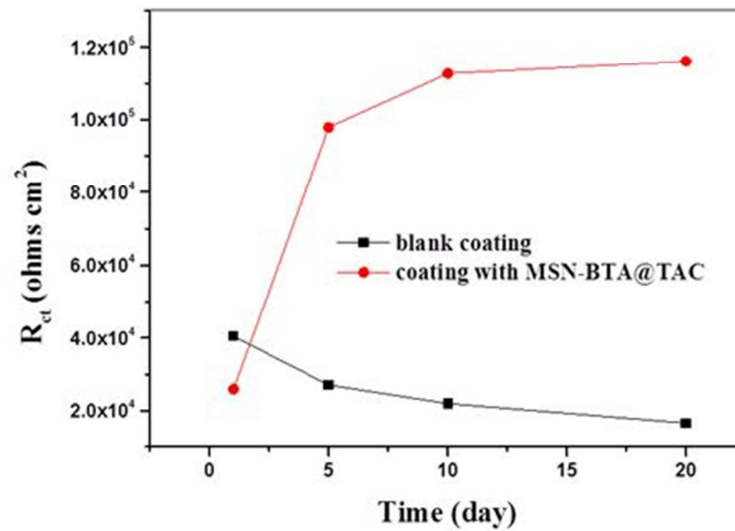


Fig. 11. R_{ct} evolution for blank coating and coating with MSN-BTA@TAC.

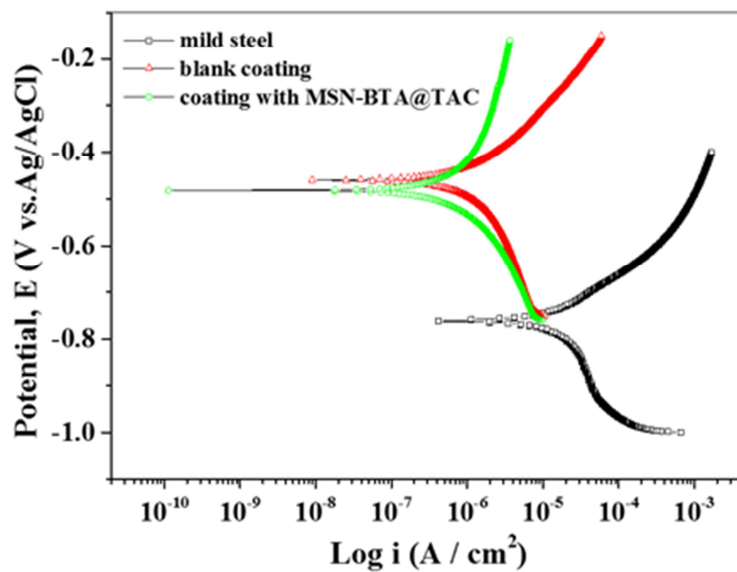


Fig. 12. Tafel plots of the mild steel (black) and scratched coatings after 20 days immersion: blank coating (red) and coating with MSN-BTA@TAC (green).

Usually, coatings with high ohmic resistance are not suitable for detection by polarization curves, because of the big difference in potential drop between the coating matrix and coating/substrate interface. In our case, the Tafel plots were taken for scratched coating after 20 days immersion. We suppose the scratched area along with the micropores will make a significant contribution to the polarisation data. Figure 12 reveals that the free corrosion potential (E_{corr}) values of scratched coatings shifts to a more positive direction as compared to the mild steel. The addition of MSN-BTA@TAC has a positive effect on both anodic and cathodic parts of the Tafel plot, especially the anodic part. The anodic Tafel slope of the coating with nanocontainers is more significant as compared to the blank coatings. The variation of the anodic branch can be ascribed to the deposition of tannic complexes to form a protective film. The values of corrosion current density (i_{corr}), anodic Tafel slope and cathodic Tafel slope were not given due to the uncertainty of the scratched area exposed to the electrolyte. It can be seen in Fig. 12 that the i_{corr} of coating with MSN-BTA@TAC decreased to less than 10^{-6} A/cm². The Tafel curves have also proved the self-healing ability of the embedded nanocontainers.

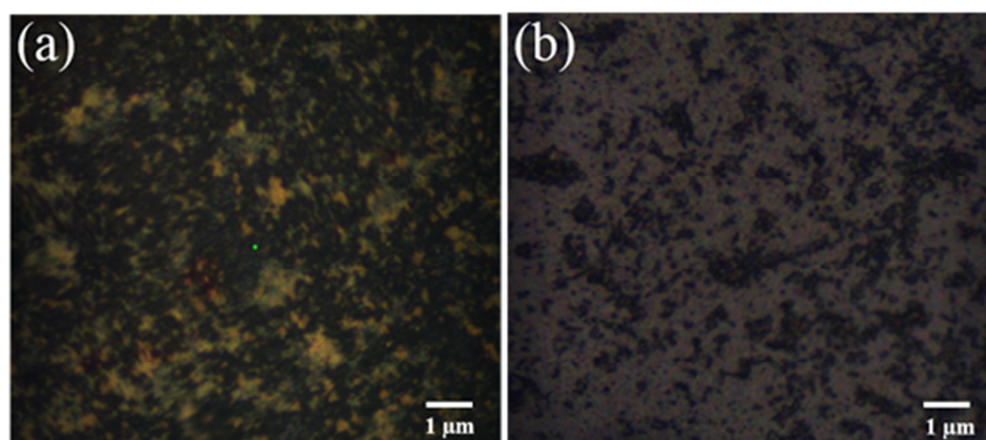


Fig. 13. Blank coating (a) and coating with MSN-BTA@TAC (b) images taken by optical microscopy after 20 days of immersion.

Because of the natural color of rust, we choosed optical microscope to observe the corrosion morphology of the coating after 20 days of immersion in 0.1 M NaCl solution. Under the magnification, rust with yellow color could be found in the unscratched area of the blank coating (Fig. 13 (a)). Fig. 13 (b) shows some dark complexes inside the micropores with MSN-BTA@TAC nanocontainers.

Nanocontainer-based self-healing coatings have been developed under the lead of Prof. Möhwald for more than ten years [33]. In this paper, we mainly focused on the design of multifunctional gatekeeper on the surface of MSNs. The protective mechanism of self-healing coatings is shown in Figure 14. As mentioned above, in addition to controlling the release of corrosion inhibitors, another advantage of the TA is their chemical reaction with rust, which leads to a more stable black ferric tannate on the surface of the steel. Corrosion protection mechanism of our coating system could be explained as follows. In the scratched area, the corrosion process will trigger the release of loaded BTA from the nanocontainers, which will provide corrosion inhibiting effect in the scratch area. TAC effectively restricts the BTA release at neutral pH for undamaged coatings. In the micropores of the coating, tannic acid detached from the shell prevent the corrosion process by the complexation with the iron ions. For more detailed description of the reaction mechanism between TA and rust, we recommend our previous paper [32].

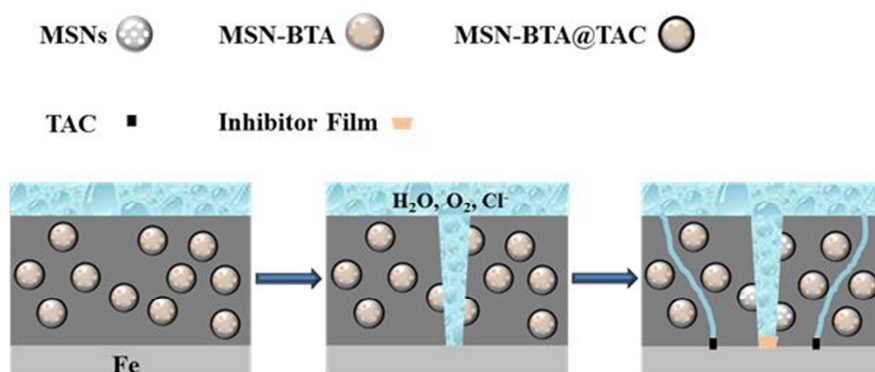


Fig. 14. Protective mechanism of self-healing coatings with MSN-BTA@TAC.

4. Conclusions

In conclusion, we demonstrated a novel controlled release benzotriazole loaded nanocontainers by using the TA-Fe (III) complex (TAC) as the shell. The deposition of TAC as a shell for BTA-loaded nanocontainers takes only 20 s. Impregnation of these nanocontainers into water-borne alkyd coatings provided them self-healing functionality for corrosion protection. The monodisperse distribution of nanocontainers inside the coating film was confirmed by SEM cross-section images. The EIS results allow us to recognize the self-healing effect clearly. The impedance of blank coating presented the downward trend during 20 days. In terms of coatings with MSNs-BTA@TAC, the impedance modulus at 0.01 Hz increased from $4.7 \times 10^4 \Omega \text{ cm}^2$ to $1.8 \times 10^5 \Omega \text{ cm}^2$. Both the released BTA and the detached TA from the surface of MSNs are contributed to the self-healing effect of the coatings MSNs-BTA@TAC. We believe our work would trigger an interest for researchers to explore multifunctional gatekeepers for core-shell nanocontainers both in intelligent anticorrosive coatings and other fields. The proposed gatekeeper for the nanocontainers can be easily up-scaled to industrial level considering their price advantage and eco-friendly characteristics.

Acknowledgments

The work was financially supported by Natural Science Foundation of China (51801110), Shandong Province Natural Science Foundation, China (ZR2017BD038, ZR2016DM21), Research Foundation for Distinguished Scholars of Qingdao Agricultural University (663-1115017).

Reference

- [1] Z. Zheng, M. Schenderlein, X. Huang, N.J. Brownbill, F. Blanc, D.G. Shchukin, Influence of Functionalization of Nanocontainers on Self-Healing Anticorrosive Coatings, *ACS Appl. Mat. Interfaces* 7(2015) 22756-22766.
- [2] D. Borisova, H. Möhwald, D.G. Shchukin, Mesoporous Silica Nanoparticles for Active Corrosion Protection, *ACS Nano*, 5 (2011) 1939-1946.
- [3] D. Borisova, D. Akçakayiran, M. Schenderlein, H. Möhwald, D.G. Shchukin, Nanocontainer-Based Anticorrosive Coatings: Effect of the Container Size on the Self-Healing Performance, *Adv. Funct. Mater.* , 23 (2013) 3799-3812.
- [4] M. Hollamby, D. Fix, I. Dönch, D. Borisova, H. Möhwald, D.G. Shchukin, Hybrid Polyester Coating Incorporating Functionalized Mesoporous Carriers for the Holistic Protection of Steel Surfaces, *Adv. Mater.* , 23 (2011) 1361-1365.
- [5] Z. Zheng, X. Huang, D.G. Shchukin, A cost-effective pH-sensitive release system for water source pH detection, *Chem. Commun.* , 50 (2014) 13936-13939.
- [6] D.V. Andreeva, D. Fix, H. Möhwald, D.G. Shchukin, Buffering polyelectrolyte multilayers for active corrosion protection, *J. Mater. Chem.* , 18 (2008) 1738-1740.
- [7] Z. Zheng, X. Huang, M. Schenderlein, H. Moehwald, G.K. Xu, D.G. Shchukin, Bioinspired nanovalves with selective permeability and pH sensitivity, *Nanoscale*, 7 (2015) 2409-2416.

- [8] W. Cheng, J. Nie, L. Xu, C. Liang, Y. Peng, G. Liu, T. Wang, L. Mei, L. Huang, X. Zeng, pH-Sensitive Delivery Vehicle Based on Folic Acid-Conjugated Polydopamine-Modified Mesoporous Silica Nanoparticles for Targeted Cancer Therapy, *ACS Appl. Mat. Interfaces* 9(2017) 18462-18473.
- [9] Z. Zheng, X. Huang, M. Schenderlein, D. Borisova, R. Cao, H. Möhwald, D.G. Shchukin, Self-Healing and Antifouling Multifunctional Coatings Based on pH and Sulfide Ion Sensitive Nanocontainers, *Adv. Funct. Mater.* , 23 (2013) 3307-3314.
- [10] T. Chen, J.J. Fu, An intelligent anticorrosion coating based on pH-responsive supramolecular nanocontainers, *Nanotechnology*, 23 (2012).
- [11] T. Chen, J.J. Fu, pH-responsive nanovalves based on hollow mesoporous silica spheres for controlled release of corrosion inhibitor, *Nanotechnology*, 23 (2012).
- [12] F. Ponzio, J. Barthès, J. Bour, M. Michel, P. Bertani, J. Hemmerlé, M. d'Ischia, V. Ball, Oxidant Control of Polydopamine Surface Chemistry in Acids: A Mechanism-Based Entry to Superhydrophilic-Superoleophobic Coatings, *Chem. Mater.* , 28 (2016) 4697-4705.
- [13] L. Zhang, J. Wu, Y. Wang, Y. Long, N. Zhao, J. Xu, Combination of Bioinspiration: A General Route to Superhydrophobic Particles, *J. Am. Chem. Soc.* , 134 (2012) 9879-9881.
- [14] N.T. Tran, D.P. Flanagan, J.A. Orlicki, J.L. Lenhart, K.L. Proctor, D.B. Knorr, Polydopamine and Polydopamine–Silane Hybrid Surface Treatments in Structural Adhesive Applications, *Langmuir*, 34 (2018) 1274-1286.
- [15] H. Lee, S.M. Dellatore, W.M. Miller, P.B. Messersmith, Mussel-Inspired Surface Chemistry for Multifunctional Coatings, *Science*, 318 (2007) 426-430.
- [16] J.H. Ryu, P.B. Messersmith, H. Lee, Polydopamine Surface Chemistry: A Decade of Discovery, *ACS Appl. Mat. Interfaces* 10 (2018) 7523-7540.

- [17] S. Chen, Y. Chen, Y. Lei, Y. Yin, Novel strategy in enhancing stability and corrosion resistance for hydrophobic functional films on copper surfaces, *Electrochem. Commun.* , 11 (2009) 1675-1679.
- [18] H.S. Hyeon, H. Seonki, R. Myung-Hyun, C.J. Wook, K.S. Min, L. Haeshin, Sprayable Ultrafast Polydopamine Surface Modifications, *Advanced Materials Interfaces*, 3 (2016) 1500857.
- [19] Q. Wei, F. Zhang, J. Li, B. Li, C. Zhao, Oxidant-induced dopamine polymerization for multifunctional coatings, *Polymer Chemistry*, 1 (2010) 1430-1433.
- [20] H. Ejima, J.J. Richardson, K. Liang, J.P. Best, M.P. van Koeveden, G.K. Such, J. Cui, F. Caruso, One-Step Assembly of Coordination Complexes for Versatile Film and Particle Engineering, *Science*, 341 (2013) 154-157.
- [21] S. Feliu, J.C. Galván, S. Feliu, J.M. Bastidas, J. Simancas, M. Morcillo, E.M. Almeida, An electrochemical impedance study of the behaviour of some pretreatments applied to rusted steel surfaces, *Corros. Sci.* , 35 (1993) 1351-1358.
- [22] S. Nasrazadani, The application of infrared spectroscopy to a study of phosphoric and tannic acids interactions with magnetite (Fe_3O_4), goethite ($\alpha\text{-FeOOH}$) and lepidocrocite ($\gamma\text{-FeOOH}$), *Corros. Sci.* , 39 (1997) 1845-1859.
- [23] T.K. Ross, R.A. Francis, The treatment of rusted steel with mimosa tannin, *Corros. Sci.* , 18 (1978) 351-361.
- [24] K. Zhang, L. Wang, W. Sun, G. Liu, Corrosion inhibitor embedded spherical micro-pits fabricated using cetyltrimethyl ammonium bromide as etching template for self-healing corrosion protection, *Corros. Sci.* , 88 (2014) 444-451.
- [25] W. Wang, L. Xu, H. Sun, X. Li, S. Zhao, W. Zhang, Spatial resolution comparison of AC-SECM with SECM and their characterization of self-healing performance of

hexamethylene diisocyanate trimer microcapsule coatings, *Journal of Materials Chemistry A*, 3 (2015) 5599-5607.

[26] B. Qian, Z. Song, L. Hao, W. Wang, D. Kong, Self-Healing Epoxy Coatings Based on Nanocontainers for Corrosion Protection of Mild Steel, *J. Electrochem. Soc.* , 164 (2017) C54-C60.

[27] B. Qian, Z. Song, L. Hao, H. Fan, Entrapment of polyaspartic acid on silica nanoparticle for self-healing coatings, *Mater. Corros.* , 68 (2017) 717-724.

[28] J.-B. Xu, Y.-Q. Cao, L. Fang, J.-M. Hu, A one-step preparation of inhibitor-loaded silica nanocontainers for self-healing coatings, *Corros. Sci.* , 140 (2018) 349-362.

[29] T.-W. Kim, P.-W. Chung, V.S.Y. Lin, Facile Synthesis of Monodisperse Spherical MCM-48 Mesoporous Silica Nanoparticles with Controlled Particle Size, *Chem. Mater.* , 22 (2010) 5093-5104.

[30] G. Grundmeier, W. Schmidt, M. Stratmann, Corrosion protection by organic coatings: electrochemical mechanism and novel methods of investigation, *Electrochim. Acta* 45 (2000) 2515-2533.

[31] M. Michailidis, I. Sorzabal-Bellido, E.A. Adamidou, Y.A. Diaz-Fernandez, J. Aveyard, R. Wengier, D. Grigoriev, R. Raval, Y. Benayahu, R.A. D'Sa, D. Shchukin, Modified Mesoporous Silica Nanoparticles with a Dual Synergetic Antibacterial Effect, *ACS Appl. Mat. Interfaces* 9(2017) 38364-38372.

[32] B. Qian, B. Hou, M. Zheng, The inhibition effect of tannic acid on mild steel corrosion in seawater wet/dry cyclic conditions, *Corros. Sci.* , 72 (2013) 1-9.

[33] D.G. Shchukin, M. Zheludkevich, K. Yasakau, S. Lamaka, M.G.S. Ferreira, H. Möhwald, Layer-by-Layer Assembled Nanocontainers for Self-Healing Corrosion Protection, *Adv. Mater.* , 18 (2006) 1672-1678.